OPTICA

Spatiotemporal refraction of light in an epsilon-near-zero indium tin oxide layer: frequency shifting effects arising from interfaces

Justus Bohn,[1,*] Ting Shan Luk,[2,3] Simon Horsley,[1] and Euan Hendry[1]

[1]School of Physics, University of Exeter, Exeter, UK
[2]Sandia National Laboratories, Albuquerque, New Mexico 87123, USA
[3]Center for Integrated Nanotechnologies, Sandia National Laboratories, Albuquerque, New Mexico 87123, USA
*Corresponding author: jb933@exeter.ac.uk

Received 12 July 2021; revised 11 October 2021; accepted 26 October 2021; published 8 December 2021

When light travels through a medium in which the refractive index is rapidly changing with time, the light will undergo a shift in its frequency. Significant frequency shifting effects have recently been reported for transparent conductive oxides. These observations have been interpreted as emerging from temporal changes to the propagation phase in a bulk medium resulting from temporal variations in the refractive index. It is an effect referred to as temporal refraction. Here, we show that the frequency shift in an epsilon-near-zero layer made of indium tin oxide originates not only from this bulk response but includes a significant effect resulting from temporal changes to the spatial boundary conditions. This boundary effect can lead to a dominant, opposing shift to the bulk effect for certain angles. Hence, this process gives rise to a frequency shift that can be tailored through the angle, decoupling the amplitude and phase modulation.

https://doi.org/10.1364/OPTICA.436324

1. INTRODUCTION

All-optical signal processing requires the control of various parameters of light waves such as amplitude, phase, and frequency. Recent work has painted a promising picture for all-optical switching, showing sub-ps and large amplitude modulation for various platforms based on amorphous silicon [1], gallium phosphide [2], plasmonic waveguides [3], and epsilon near zero (ENZ) layers [4–6], including indium tin oxide (ITO) [7,8]. Even cavity-based optical transistors have been demonstrated [9,10]. However, while the amplitude of light can be straightforwardly controlled using these different modulator materials, controlling the frequency of light is more challenging. Control over the frequency is required for applications such as laser tuning, temporal [11], and spectral [12] pulse compression and optical switching of channels in telecomunications [13]. Meanwhile, the ability to control both the amplitude and frequency of a wave independently is thought to be important to generate the spatiotemporal modulation required for nonreciprocal devices [14] and time crystals [15]. To modulate the frequency of an optical signal, one can change its phase on ultrafast time scales, effectively creating a temporal refractive index boundary [16–18]. However, in many circumstances, changes to frequency are necessarily and directly coupled to changes in amplitude, making independent modulation difficult.

Recently, thin films of ENZ materials have offered a promising route to frequency modulation [19–22]. In such materials, significant (>unity) changes to the refractive index can be induced on sub-100 fs timescales due to ultrafast heating of the electron gas [5,7], an effect which can result in frequency shifts by up to a few percent of the carrier frequency [20]. However, while observed frequency shifts are large when temporal refraction occurs in these systems, they are also directly linked to refractive index changes, which leads to simultaneous amplitude modulation, preventing independent optimization.

Here, we investigate spatiotemporal refraction for tailored frequency shifting in thin ITO layers. We show that the frequency shift arises not only from a bulk response but includes a significant contribution from temporal changes to the spatial boundary conditions. The frequency shift arising from boundary effects can oppose the bulk effect and can even be the dominant contribution for sub-μm layer thicknesses. We further show that for high incident angles, it gives rise to a dominant, opposing shift (i.e., shifting to higher rather than the usual lower frequencies), while maintaining an increase in differential transmission. This competition between surface and bulk responses could have applications where tuning the amplitude and direction of frequency shift is useful, or decoupling of amplitude and phase modulation is required.

2. RESULTS

A. Temporal Changes to Phase

For temporal refraction, a bulk medium of homogeneous refractive index n undergoes a temporal change in index [23]. The temporal

shape of the phase change is determined by the nonlinear refractive index change $\Delta n = n_2 I$, which depends on the nonlinear material characteristics n_2 and the pump pulse intensity I. Time translation symmetry breaking leads to a change in frequency Δf, determined by $nf = (n + \Delta n)(f + \Delta f)$, predicting that the fractional frequency shift $\Delta f/f$ should depend only on the material indices through $\Delta n/(n + \Delta n)$.

However, nonlinear media can be considerably thinner than the spatial extent of a laser pulse, so only a part of a pulse is present in the medium at any one moment in time. Under such conditions, the time translation symmetry argument outlined above breaks down. This is particularly true for films of ITO, which are highly absorptive close to the ENZ frequency, so that transmission is very low for film thicknesses >1 μm. When films of several hundred nanometer thickness are excited by femtosecond pulses, the frequency shifts measured in experiments are considerably smaller than those predicted by time translation symmetry breaking [20]. Under these circumstances, one should instead calculate time-dependent changes to the transmitted phase of the laser pulse. Consider the change in phase for normal incidence, arising from propagation through the bulk of the film. For a time-dependent change to index $\Delta n(t)$ one predicts a change in phase given by $\Delta\Phi(t) = \Delta n(t) k_0 d$ (see Fig. 1), where k_0 is the wavenumber of the incident radiation in free space. We see from this that the thickness of the film d is expected to limit the phase change, and therefore the observable frequency shift, which is determined by

$$\Delta\omega = -\mathrm{d}\Phi/\mathrm{d}t. \tag{1}$$

However, in thin films, interfaces also play an important role in determining the transmission phase. Effects arising from a temporal change of the Fresnel coefficients describing interfaces have been suggested to contribute to frequency shifting [21], and are expected to be independent of the film thickness. When the complex ITO refractive index, or equivalently permittivity ε, varies with time, as in Fig. 2(a), the Fresnel coefficients for the interface of the ITO will also vary with time. This will result in time-dependent spatial refraction at the interface, referred to here as spatiotemporal refraction. The temporal change to this boundary-induced phase can be associated with a frequency shift, as per Eq. (1) above, alongside the temporal refraction induced by the bulk.

We can predict temporal changes to the ITO thin layer transmission coefficient (t_{13}) using the Airy formula, given as

$$t_{13} = \frac{1}{1 + r_{12} r_{23} \mathrm{e}^{2ik_2 d}} t_{12} t_{23} \mathrm{e}^{ik_2 d}, \tag{2}$$

with the Fresnel coefficients of the front (r_{12}, t_{12}) and back interface (r_{23}, t_{23}). Here, we treat the time-dependent changes to

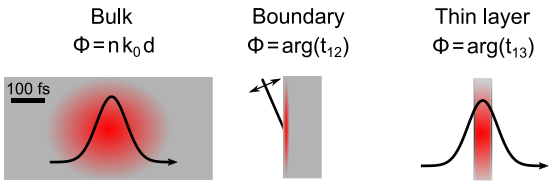

Fig. 1. Temporal changes in an optical medium. The schematic of the bulk propagation case highlights that the nonlinear refractive index facilitates a temporally changing phase for intense laser pulses. The Fresnel coefficients can be used to extract phase changes at a spatial boundary. Temporal changes to the interface induced phase jumps also shift the frequency. Finally, the thin layer case studied in this letter, which combines these phenomena.

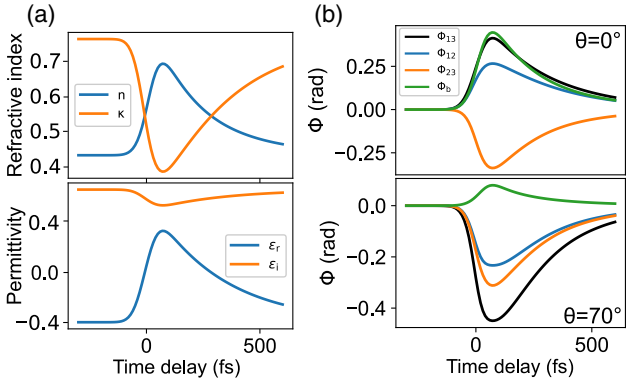

Fig. 2. Spatiotemporal refraction simulation. We study the impact of a typical ω_p reduction by 10% for the 407 nm ITO sample parameters at 200 THz. (a) Upper panel shows that the real part of the refractive index n initially increases until the electron gas reaches the minimum ω_p, while the imaginary part κ decreases. They cross roughly at the maximum gradient, corresponding to the ENZ point as seen below for the real part of the permittivity being zero (ε_r). The thermal decay is modeled with a time constant of 300 fs, as described in Supplement 1, Sections S1 and S2. The lower panel presents the same changes in terms of permittivity. (b) For the case of normal incidence, the simulated thin layer transmission phase (Φ_{13}) agrees very well with the bulk phase ($\Phi_b = k_2 d$). However, for an incoming angle of 70° a total thin layer phase shift of opposite sign is expected.

permittivity as being homogeneous throughout the ITO layer. In Supplement 1, Section S3, we will revisit this assumption and show that spatial in-homogeneity due to the exponential decay of the pump throughout the sample leads to relatively minor quantitative differences. For non-normal incidence at angle θ, we label the angle of the wavevector inside the ITO layer as θ_2. Then, the bulk phase change (Φ_b) is determined by the multiplication of the ITO thickness (d) and the normal wavevector component inside the ITO layer ($k_2 = nk_0 \cos\theta_2$). Further phase contributions appear from the Fresnel transmission coefficients (Φ_{12}, Φ_{23}) and the internal reflections term $\Phi_{ir} = \arg(1/(1 + r_{12} r_{23} \mathrm{e}^{2ik_2 d}))$.

We consider a beam incident from air, followed by an ITO layer (sample details in Supplement 1, Section S1), followed by a glass substrate. Excitation of such a system near the ENZ frequency heats the electron gas, introducing strong optical nonlinearity thought to arise predominately from changes to plasma frequency [5,7]. To gain qualitative insights into the expected behavior, we define temporal changes to the bulk plasma frequency as a convolution of our Gaussian pump pulse, with a pulse length of 107 fs, and an exponential decay of 300 fs, determined from optical pump-probe measurements using the analysis presented in [8]. For a sample with an ENZ frequency at 211.5 THz, undergoing an estimated 10% red shift of the plasma frequency ω_p, a probe frequency $f_{pr} = 200$ THz will experience the temporal changes to permittivity and refractive index plotted in Fig. 2(a). For such a red shifting ω_p, the real part of the refractive index n initially increases on pumping, while the imaginary part initially decreases. For the plotted example, the real part of the permittivity crosses zero shortly after pumping, which corresponds to the ENZ condition.

Using Eq. (2), and for a sample with $d = 407$ nm, we can extract the transmission coefficient of our thin layer based on the time-dependent refractive index and plot the corresponding phase in Fig. 2(b). For normal incidence (upper panel), we see that the phase change due to the interfaces, Φ_{12} and Φ_{23}, are opposite in

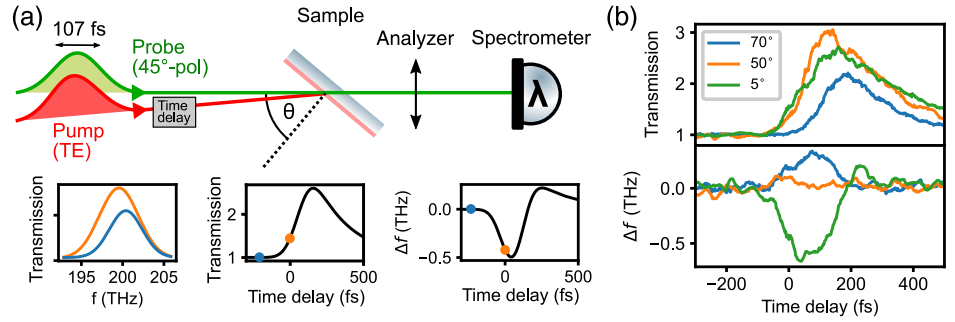

Fig. 3. Experimental setup and measurement. (a) Setup consists of a TE polarized pump and a 45° probe that enables quick spectral measurement of either polarization by choice of the analyzer. The samples of interest are ITO films of 407 nm or 115 nm thickness on top of a coverslip. The lower plots show schematically how the measured spectra (left) at different time delays (blue, orange) can be used to extract changes in both transmission (middle) and central frequency (left). (b) Measurements taken for three different angles. They correspond to an incident pump intensity of $I_0 = 400\ \mathrm{GW\ cm^{-2}}$, $f_{\mathrm{pm}} = 250$ THz, $f_{\mathrm{pr}} = 200$ THz, and TM polarization. The transmission increases up to 200 to 300% for all angles, while the frequency shift is either negative (5°), negligible (50°), or positive (70°).

sign and approximately cancel. The resulting total time-dependent phase for this normal case, Φ_{13}, is then similar to that predicted from Φ_{b}, the change in phase expected due to propagation through the bulk.

However, increasing the angle of incidence leads to a very different phase response. For larger angles, the temporal gradient of the transmission phase can even change sign, as seen in the example of 70° incidence presented in the lower panel of Fig. 2(b). This behavior arises due to the interface contributions, which no longer cancel each other. Moreover, these interface contributions also lead to a change in phase that is opposite in sign to the to normal incidence case; i.e., a decrease in phase for the permittivity transitioning from negative to positive real values. This effect is fundamentally different from the bulk response, demonstrating the importance of the interfaces in determining changes in phase and frequency. Interestingly, such a contrasting behavior of the phase results in an apparent experimental signature: a blue shift of the frequency instead of the red shift expected from a bulk. A more in-depth guide to understand the model, the individual contributions, and the different limits can be found in Supplement 1, Section S2.

B. Experimental Measurement

To experimentally investigate this signature, we carry out a pump-probe measurement as depicted in Fig. 3(a), defined by the parameters I_0 (the peak intensity of the pump pulse in the incident air), f_{pm} (the central frequency of the pump pulse), and f_{pr} (the central frequency of the probe pulse). Unless otherwise stated, we use $I_0 = 400\ \mathrm{GW\ cm^{-2}}$, resulting in frequency red shifts of 1 THz. We note that our observed frequency shifts reported below are lower than those reported in [20]. This is due to a higher Drude scattering rate and a reduced thickness for our ITO samples.

A TE pump polarization is chosen because it provides only a slight angle and frequency dependence in absorption. We use a probe polarized at 45° to check the frequency shifting behavior of either polarization by rotating an analyzer in front of a spectrometer. Spectra are recorded for different pump delay times. The spectra form the data basis, which we translate into changes in frequency and transmission of the central frequency of the pulse, both presented relative to the initial probe spectrum without pumping. The experimental data plotted in Fig. 3(b) show typical behavior for a probe frequency slightly below the initial ENZ frequency: a strong initial increase of the transmission as a function of time for all three angles (5°, 50°, 70°), up to 300% of the initial transmission. Simultaneously, very different frequency shifting effects are measured: For the low angle case (5°), the typical red shifting behavior is observed, while the high angle case (70°) presents a blue shift; as described above, this is a signature dominated by the change in phase at the interface. This interface effect can act as an opposing shift and may be used to tailor the frequency shift or even suppress it entirely, as seen for 50°.

C. Thickness Dependence

Intuitively, one would expect the effect of interfaces to be more important for thinner samples. To investigate this, we repeat the initial predictions shown in Fig. 2 for a varying thickness of ITO. In Fig. 4(a), we plot the maximal frequency shift for the red shift feature ($\theta = 0°$) and blue shift feature ($\theta = 70°$) as a function of ITO thickness, predicted using the quasi-time harmonic model introduced below. The red shift feature is predicted to scale linearly with the thickness of the sample, which is in line with expectations that the signal is predominantly determined by the bulk phase. However, the high angle blue shift feature is dominated by surface effects, and is relatively thickness independent for $d > 200$ nm. For $d < 200$ nm, internal reflections counteract the blue shift, leading to a gradual decrease of the shift as $d \to 0$ (also see Supplement 1, Figure S3). For very thick films with $d > 1000$ nm, the blue shift again decreases through the counteracting bulk contribution, which is comparatively small for large angles, since $\Phi_{\mathrm{b}} \propto \cos(\theta_2)$.

To demonstrate this effect experimentally, we compare the measured frequency shifts for the $d = 407$ nm sample [Fig. 4(b)] to a considerably thinner one with $d = 115$ nm [Fig. 4(c)]. Figure 4(c) clearly shows a strongly reduced red shift feature, agreeing with the expectation of a reduced bulk effect. Additionally, with the decline of the red shift, the blue shift feature has become more prominent. In the experiment, we observe that the frequency shift in this region is even larger than that measured for the 407 nm thick film, an effect explained primarily by a lower scattering rate for this particular sample.

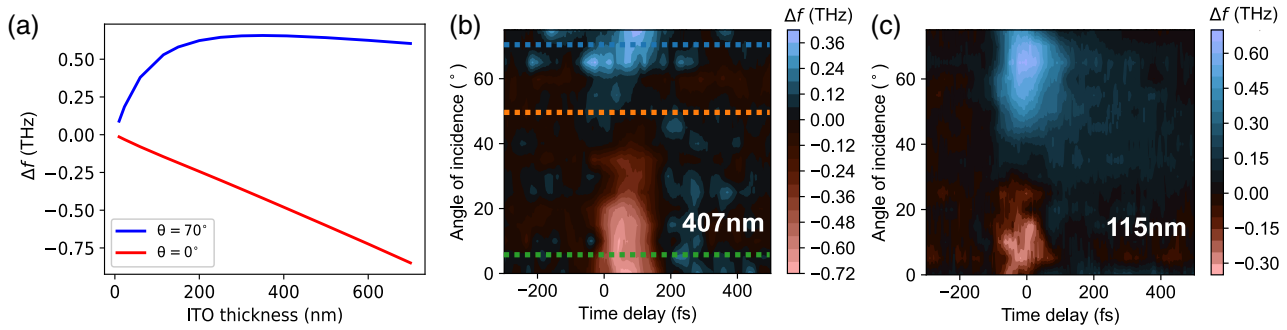

Fig. 4. Thickness dependence. (a) To further investigate the thickness dependence, we model the ITO for the two angle extremes depending on the layer size. The quickly saturating blue shift (high angle) and a linearly increasing red shift (low angle) are plotted (ω_p reduction by 10%, 417 nm sample parameters, $f_{pr} = 200$ THz). (b) Experimentally measured frequency shifts of the 407 nm layer, similar to the measurements in Fig. 3(b) with angles marked by dashed lines of the corresponding colors ($I_0 = 400$ GW cm^{-2}, $f_{pm} = 250$ THz, $f_{pr} = 200$ THz, and TM polarization). (c) Experimentally measured frequency shift of a 115 nm layer ($I_0 = 400$ GW cm^{-2}, $f_{pm} = 214$ THz, $f_{pr} = 240$ THz, and TM polarization).

D. Comparison between Experiment and Models

One can calculate the expected frequency shift by relating measured transmission changes to expected temporal changes in phase, which can then be used to predict expected frequency shifts. The simplest possible way to achieve this is using a quasi-time harmonic model, where we first calculate expected temporal changes to the permittivity of the material, relate this to expected temporal changes to transmission phase, and directly predict from this expected changes to the frequencies contained in a probe pulse using Eq. (1). This is possible via the following steps: First, we use a standard pump-probe measurement to determine the temporal dynamics of transmission amplitude versus time, which we fit using the convolution of a Gaussian and exponential decay. We then calculate t_{13} for a given incident frequency f and angle θ via Eq. (2) for different bulk plasma frequencies. The results from this calculation are used as a spline function to convert the measured change in the amplitude of transmission into corresponding changes of the bulk plasma frequency. We then convert from plasma frequency versus time to transmission phase versus time, again using Eq. (2). Finally, we calculate the temporal derivative of the extracted phase, and use this to estimate the expected frequency shift as per Eq. (1). Note that this model assumes all frequencies in the pulse respond identically; hence, we refer to it as quasi-time harmonic and we come back to this approximation later.

The frequency shifts predicted by this quasi-time harmonic model are shown in Fig. 5(a). The qualitative behavior predicted in Fig. 5(a), defined by the relative amplitudes of red- and blue-frequency shifts, as well as the angle at which the frequency shift changes sign, is in good agreement with our direct measurement in Fig. 4(b). This is striking, especially considering there are no fitting parameters used in our approach. For this simple quasi-time harmonic model, we expect the most significant frequency shifts to occur at the times corresponding to the maximal change in the optical properties of the material. As shown in Fig. 5(c) (blue line), we see the maximum in predicted frequency shift corresponds to the maximum temporal gradient in index [blue arrow in Fig. 5(c)]. This can also be seen in Fig. 3(b), where the largest frequency shifts are measured for the largest slope of the transmission change. Similarly, we expect zero frequency change for the times corresponding to zero gradient in index, as seen for the time corresponding to the extremum in plasma frequency (red arrow). These two behaviors explain the narrow temporal widths of the frequency shift features seen in both the model [Fig. 5(a)] and the experiment [Fig. 4(b)].

Nevertheless, we note that there are some approximations used in our quasi-time harmonic modelling approach. First, the finite penetration depths of the laser pulses results in an in-homogeneous refractive index of the ITO throughout the thickness of the film. We can take this effect into account by treating the ITO as a multilayer structure, with the index change in each layer determined by the predicted pump intensity in that layer, as described in detail in Supplement 1, Section S3. The resulting prediction shown in Fig. 5(b), while qualitatively very similar, predicts a smaller blue shift and larger red shift than the single-layer model presented in Fig. 5(a), in better agreement with the measurement in Fig. 4(b).

For changes in refractive index that occur on the timescale of the oscillating field, one should also convolve the probe field with the time-dependent response of the medium. This approach, which describes the full temporal dynamics of the interaction including the broadband nature of the probe pulse, is discussed in detail in Supplement 1, Section S4. As shown in Fig. 5(c), this full temporal model (orange line) shows only a small difference in terms of the maximum predicted frequency shift. However, the response is slightly broadened in time compared to that predicted by the quasi-time harmonic response, curtailing the negative frequency shift seen previously for times beyond 200 fs, which is again more similar to the observation in the experiment in Fig. 4(b). This can be understood to arise from two effects: First, the temporal width of the probe pulse spreads the frequency shifting event in time. Second, the Gaussian frequency distribution of the probe pulse is reshaped not only by spatiotemporal refraction but also by the temporally shifted spectral absorption peak of the ITO layer. This last point is often ignored, but very important for absorbing materials, where it can be difficult to separate changes in the absorption of the material from effects arising from the temporal gradient in index. For example, in Fig. 5(d) we see that the spectrum corresponding to the maximal frequency shift (blue line) does not correspond to the maximum change in transmission intensity (red line). In such circumstances where the frequency shifts are small, the two main signatures discussed above (i.e., the observation of the maximum shift corresponding to maximum gradient in index, and the change in sign of frequency shift with angle) are both clear indications that can help distinguish spatiotemporal refraction.

Finally, we point out that a complete model that simultaneously takes into account both the convolution between the temporal

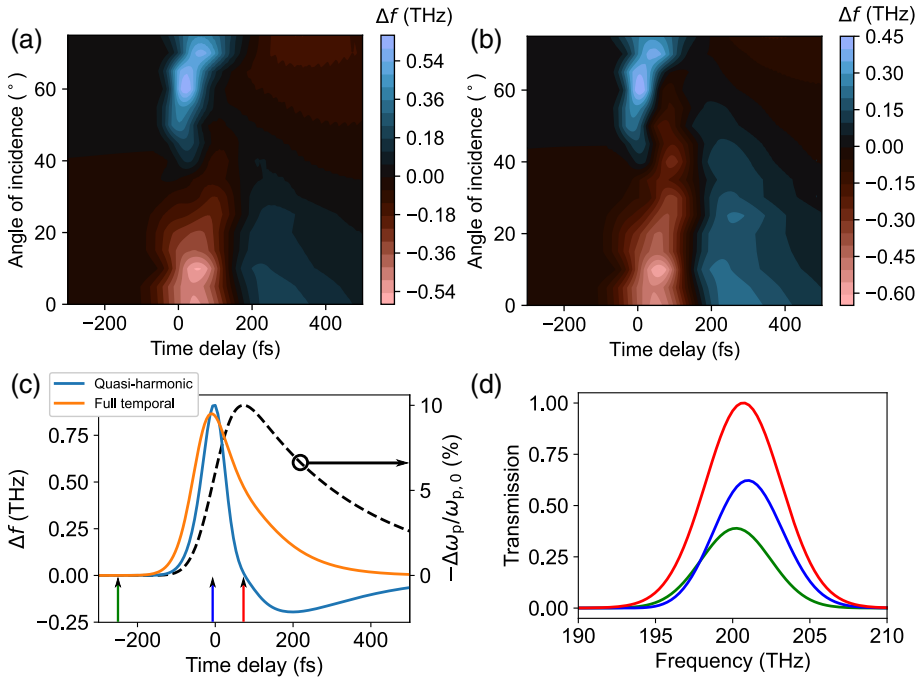

Fig. 5. Modeling of experimental data. Predicted frequency shifts under the quasi-time harmonic approximation (see text) assuming (a) homogeneous and (b) inhomogeneous layer approximations, calculated assuming parameters: ($I_0 = 400$ GW cm^{-2}, $f_{pm} = 250$ THz, $f_{pr} = 200$ THz, and TM polarization). (c) Comparison between the quasi-time harmonic (blue solid) and the full temporal (orange solid) model, described in detail in Supplement 1, Section S4. The temporal response of the optical material assumes a reduction in plasma frequency of 10% (dashed black). The full temporal model takes into account the spectral width of 5.3 THz FWHM. The times marked by arrows correspond to: before interaction (green), maximum gradient in index (blue), and zero gradient in index (red). (d) Frequency distributions corresponding to the three marked times in (c), as predicted by the full temporal model. Modeled frequency shifts are lower than those reported in [20] due to a higher Drude scattering rate and a reduced thickness in our samples.

dynamics and the field, as well as the complete spatial dependence of the refractive index, is a complex computational task and lies beyond the scope of this paper.

3. CONCLUSION

In conclusion, we show that spatiotemporal refraction provides a frequency shift that is relatively strong compared to the temporal refraction for sub-μm samples. This contribution remains roughly constant down to film thicknesses of 100 nm. Most importantly, we demonstrate that the frequency shift can now be controlled not only by the temporal refractive index changes but also by the angle. This enables tailoring the nonlinear frequency shift in thin layers independent of other nonlinear modulations such as the transmission. In future, more versatile layer choices or combining multiple layers could provide a plethora of ultrafast amplitude and frequency switching devices by tuning interface effects to obtain the desired results.

Funding. Royal Society (RPG-2016-186); U.S. Department of Energy; Engineering and Physical Sciences Research Council (EP/L015331/1).

Acknowledgment. We acknowledge financial support from the EPSRC of the United Kingdom, via the EPSRC Centre for Doctoral Training in Metamaterials. Author Ting Shan Luk acknowledges the support of the U.S. Department of Energy, Office of Basic Energy Sciences, Division of Materials Sciences and Engineering. Part of this work was performed at the Center for Integrated Nanotechnologies, an Office of Science User Facility operated for the U.S. Department of Energy (DOE) Office of Science. Author Simon Horsley acknowledges funding from the Royal Society and TATA. We thank Philip Thomas for the ellipsometry measurement of the ITO thin film. We thank Bill Barnes and Zahirul Alam for helpful discussions.

Disclosures. The authors declare no conflicts of interest.

Data availability. Data underlying the results presented in this paper are available from the University of Exeter's institutional repository at [24]. The Python codes to analyze and plot the data are included.

Supplemental document. See Supplement 1 for supporting content.

REFERENCES

1. M. R. Shcherbakov, P. P. Vabishchevich, A. S. Shorokhov, K. E. Chong, D.-Y. Choi, I. Staude, A. E. Miroshnichenko, D. N. Neshev, A. A. Fedyanin, and Y. S. Kivshar, "Ultrafast all-optical switching with magnetic resonances in nonlinear dielectric nanostructures," Nano Lett. **15**, 6985–6990 (2015).
2. G. Grinblat, M. P. Nielsen, P. Dichtl, Y. Li, R. F. Oulton, and S. A. Maier, "Ultrafast sub-30-fs all-optical switching based on gallium phosphide," Sci. Adv. **5**, eaaw3262 (2019).
3. M. Ono, M. Hata, M. Tsunekawa, K. Nozaki, H. Sumikura, H. Chiba, and M. Notomi, "Ultrafast and energy-efficient all-optical switching with graphene-loaded deep-subwavelength plasmonic waveguides," Nat. Photonics **14**, 37–43 (2020).
4. N. Kinsey, C. DeVault, J. Kim, M. Ferrera, V. M. Shalaev, and A. Boltasseva, "Epsilon-near-zero Al-doped ZnO for ultrafast switching at telecom wavelengths," Optica **2**, 616 (2015).
5. L. Caspani, R. P. Kaipurath, M. Clerici, M. Ferrera, T. Roger, J. Kim, N. Kinsey, M. Pietrzyk, A. Di Falco, V. M. Shalaev, A. Boltasseva, and D. Faccio, "Enhanced nonlinear refractive index in epsilon-near-zero materials," Phys. Rev. Lett. **116**, 233901 (2016).
6. Y. Yang, K. Kelley, E. Sachet, S. Campione, T. S. Luk, J. P. Maria, M. B. Sinclair, and I. Brener, "Femtosecond optical polarization switching using a cadmium oxide-based perfect absorber," Nat. Photonics **11**, 390–395 (2017).
7. M. Z. Alam, I. De Leon, and R. W. Boyd, "Large optical nonlinearity of indium tin oxide in its epsilon-near-zero region," Science **352**, 795–797 (2016).

8. J. Bohn, T. S. Luk, C. Tollerton, S. W. Hutchings, I. Brener, S. Horsley, W. L. Barnes, and E. Hendry, "All-optical switching of an epsilon-near-zero plasmon resonance in indium tin oxide," Nat. Commun. **12**, 1017 (2021).
9. W. Chen, K. M. Beck, R. Bücker, M. Gullans, M. D. Lukin, H. Tanji-Suzuki, and V. Vuletić, "All-optical switch and transistor gated by one stored photon," Science **341**, 768–770 (2013).
10. A. V. Zasedatelev, A. V. Baranikov, D. Urbonas, F. Scafirimuto, U. Scherf, T. Stöferle, R. F. Mahrt, and P. G. Lagoudakis, "A room-temperature organic polariton transistor," Nat. Photonics **13**, 378–383 (2019).
11. T. Gustafson, P. Kelly, and R. Fisher, "Subpicosecond pulse generation using the optical Kerr effect," IEEE J. Quantum Electron. **5**, 325 (1969).
12. S. A. Planas, N. L. P. Mansur, C. H. B. Cruz, and H. L. Fragnito, "Spectral narrowing in the propagation of chirped pulses in single-mode fibers," Opt. Lett. **18**, 699–701 (1993).
13. C. Brackett, "Dense wavelength division multiplexing networks: principles and applications," IEEE J. Sel. Areas Commun. **8**, 948–964 (1990).
14. D. L. Sounas, C. Caloz, and A. Alù, "Giant non-reciprocity at the subwavelength scale using angular momentum-biased metamaterials," Nat. Commun. **4**, 2407 (2013).
15. E. Lustig, Y. Sharabi, and M. Segev, "Topological aspects of photonic time crystals," Optica **5**, 1390–1395 (2018).
16. S. A. Akhmanov, A. P. Sukhorukov, and A. S. Chirkin, "Nonstationary phenomena and space-time analogy in nonlinear optics," Sov. Phys. JETP **28**, 748–757 (1969).
17. J. C. AuYeung, "Phase-conjugate reflection from a temporal dielectric boundary," Opt. Lett. **8**, 148–150 (1983).
18. J. T. Mendonca, *Theory of Photon Acceleration* (CRC, 2000).
19. V. Bruno, S. Vezzoli, C. De Vault, E. Carnemolla, M. Ferrera, A. Boltasseva, V. M. Shalaev, D. Faccio, and M. Clerici, "Broad frequency shift of parametric processes in epsilon-near-zero time-varying media," Appl. Sci. **10**, 1318 (2020).
20. Y. Zhou, M. Z. Alam, M. Karimi, J. Upham, O. Reshef, A. E. Willner, and R. W. Boyd, "Broadband frequency translation through time refraction in an epsilon-near-zero material," Nat. Commun. **11**, 2180 (2020).
21. J. B. Khurgin, M. Clerici, V. Bruno, L. Caspani, C. DeVault, J. Kim, A. Shaltout, A. Boltasseva, V. M. Shalaev, M. Ferrera, D. Faccio, and N. Kinsey, "Adiabatic frequency shifting in epsilon-near-zero materials: the role of group velocity," Optica **7**, 226–231 (2020).
22. C. Liu, M. Z. Alam, K. Pang, K. Manukyan, O. Reshef, Y. Zhou, S. Choudhary, J. Patrow, A. Pennathurs, H. Song, Z. Zhao, R. Zhang, F. Alishahi, A. Fallahpour, Y. Cao, A. Almaiman, J. M. Dawlaty, M. Tur, R. W. Boyd, and A. E. Willner, "Photon acceleration using a time-varying epsilon-near-zero metasurface," ACS Photon. **8**, 716–720 (2021).
23. W. R. Donaldson, G. P. Agrawal, and B. W. Plansinis, "What is the temporal analog of reflection and refraction of optical beams," Phys. Rev. Lett. **115**, 183901 (2015).
24. J. Bohn, T. S. Luk, E. Hendry, and S. Horsely, "Spatiotemporal refraction of light in an epsilon-near-zero ITO layer: frequency shifting effects arising from interfaces (dataset)," University of Exeter (2021) https://doi.org/10.24378/exe.3644.